

Supporting Information

The Cobalt Oxidation State in Preferential CO Oxidation on CoO_x/Pt(111) investigated by Operando X-ray Photoemission Spectroscopy

Eoghan Rattigan[§], Zhaozong Sun[§], Tamires Gallo[‡], Miguel Angel Nino^{‡,}, Sofia de Oliveira Parreiras[‡], Cristina Martín-Fuentes[‡], Juan Carlos Martín-Romano[‡], David Écija[‡], Carlos Escudero^{*}, Ignacio Villar^{*}, Jonathan Rodríguez-Fernández^{§,1}, Jeppe V. Lauritsen^{*§}*

[§] Interdisciplinary Nanoscience Center (iNANO), Aarhus University, Gustav Wieds Vej 14, 8000 Aarhus, Denmark

[‡] Synchrotron Radiation Research, Lund University, Sölvegatan 14, 223 62 Lund, Sweden

[‡] IMDEA Nanoscience Institute, Calle Faraday 9, Ciudad Universitaria de Cantoblanco, 28049, Madrid, Spain

^{*} ALBA Synchrotron, Carrer de la Llum 2-26, Cerdanyola del Vallès 08290, Barcelona, Spain

Section 1. Bare Pt Substrate

The bare Pt substrate was first cleaned, and exposed to a 2:1 mixture of CO and O₂ in a 2:1 ratio at CIRCE beamline ALBA¹ where AP-XPS was performed. QMS of the gas in the cell was performed, Figure S1C, allowing the light-off of the CO₂ to be seen at 250°C. The crystal was then heated from RT to 300°C, as seen in Figure S1. In Figure S1A the C1s region of the XPS spectra can be seen. Unfortunately in UHV there is still a large amount of adventitious carbon on the surface. Introducing the gas mixture sees the appearance of two surface peaks marked with the blue

dashed lines at 286.5eV and 285.8eV, assigned to the on-top and bridge adsorption sites for the CO on Pt(111)². At higher binding energy the CO gas phase peak³ can be seen, and at temperatures 250°C and above, after CO₂ light-off its gas phase peak can also be seen. Figure S1B shows the O1s region of the XPS spectra for same crystal. At room temperature in the gas mixture, multiple peaks are seen to appear, those located at higher binding energy are related to the gas phase labelled O₂(g)⁴ (split peaks) and CO(g)³. The surface peaks marked in blue are located at 530.8 eV and 532.5 eV are related to the adsorbed CO². CO_{ads} can occupy both the bridge site and the top site in a c(4 × 2) structure at the pressures present during the experiment. However these peaks are shifted to lower binding energies than reported in literature, with the 530.8 eV binding energy often reported as the value for chemisorbed oxygen (O_{ads})⁵. This occupies the hollow sites of the Pt(111) and it is the interaction with the CO in the bridge sites that is deemed crucial in the CO oxidation⁶, which the ball model in Figure S1D illustrates. The idea that there is also O in the hollow sites is collaborated by the C1s region, Figure S1A, whereby the bridge peak, has a lower intensity, in contrast to when there is no oxygen present leading to the belief that at least some of the hollow sites are occupied by O_{ads}. As the sample is heated to above 200°C, where we first see lift-off of CO₂ you can also see that the bridge site peak diminishes faster than the on-top peak, in both the O1s and C1s regions.

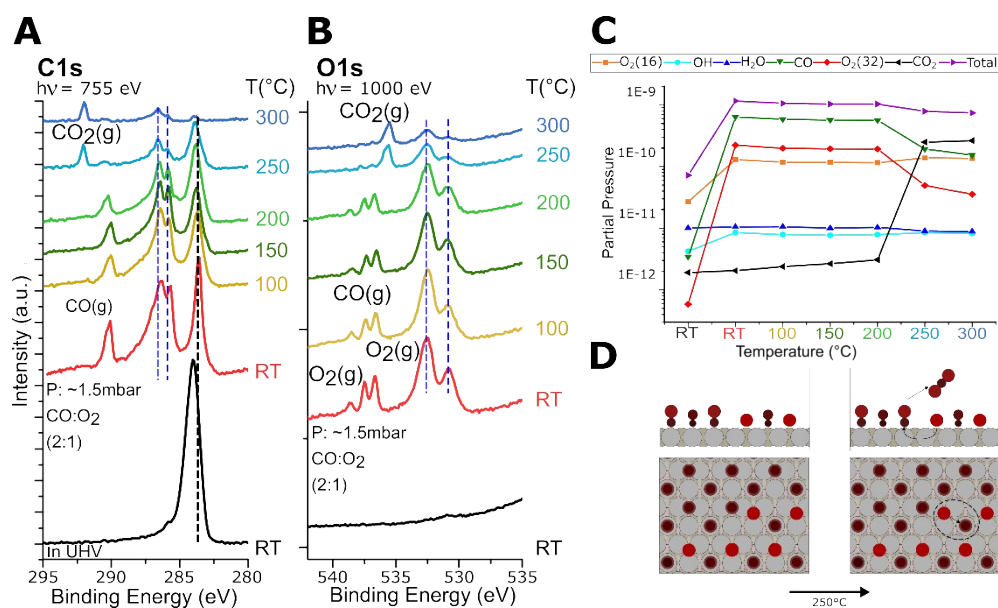


Figure S1. **A&B** show the AP-XPS spectra for the C1s and O1s regions as a Pt(111) crystal is heated from RT to 300°C in a 2:1 gas mixture of CO and O₂. **C** the QMS of the gas in the cell during the experiment. **D** a ball model of the interaction on the surface, with oxygen atoms, red, interaction with CO molecules, dark red, on the Pt(111), grey, surface.

Section 2. Fitting the Co2p peaks.

The Co2p^{3/2} region of the XPS spectra obtained at the HIPPE beamline in both CO oxidation and PROX conditions was fitted using CASA XPS⁷. A peak fit of 6 peaks was chosen in line with the work by A.J. Holt et al⁸. The first three of the 6 peaks are fitted as asymmetric peaks, as seen in Figure S2, and are the Co metal (fitting using the main asymmetrical peak at 778eV⁹), the Co³⁺ oxidation peak associated with the trilayer structure located at 778.9eV^{9,10} and the Co²⁺ oxidation peak associated with the bilayer structure of the CoO_x seen at 780.4eV. The peaks labeled I and II are peaks associated with multiplet splitting and shake-up satellites of the high-spin Co²⁺ state, and located 2.1 eV and 5.7eV away from the main peak respectively¹¹⁻¹⁴. The minor peak III is linked with Co³⁺ compounds⁸. The peak fit was energy calibrated to the Pt 4f^{5/2} peak, measured at each interval using the same photon energy, 1250eV for the Co2p region. Using the fitted peaks an approximation of the percentage make-up of the CoO_x was calculated for each temperature of each experimental series. A visual representation of this can be seen in Figure S3. The percentage

contribution presented in the main text arises from the addition of all the peaks associated with a certain oxidation state, for example for the Co^{2+} we take the main Co^{2+} peak, as well as peaks I and II which are associated with that state and for Co^{3+} it is the main peak and peak III. Note that we always see some metallic Co^0 component in all spectra even in oxidizing conditions, which we however do not consider to reflect full metallic Co species on the surface, expect at high temperature where the oxide decomposes. $\alpha\beta$

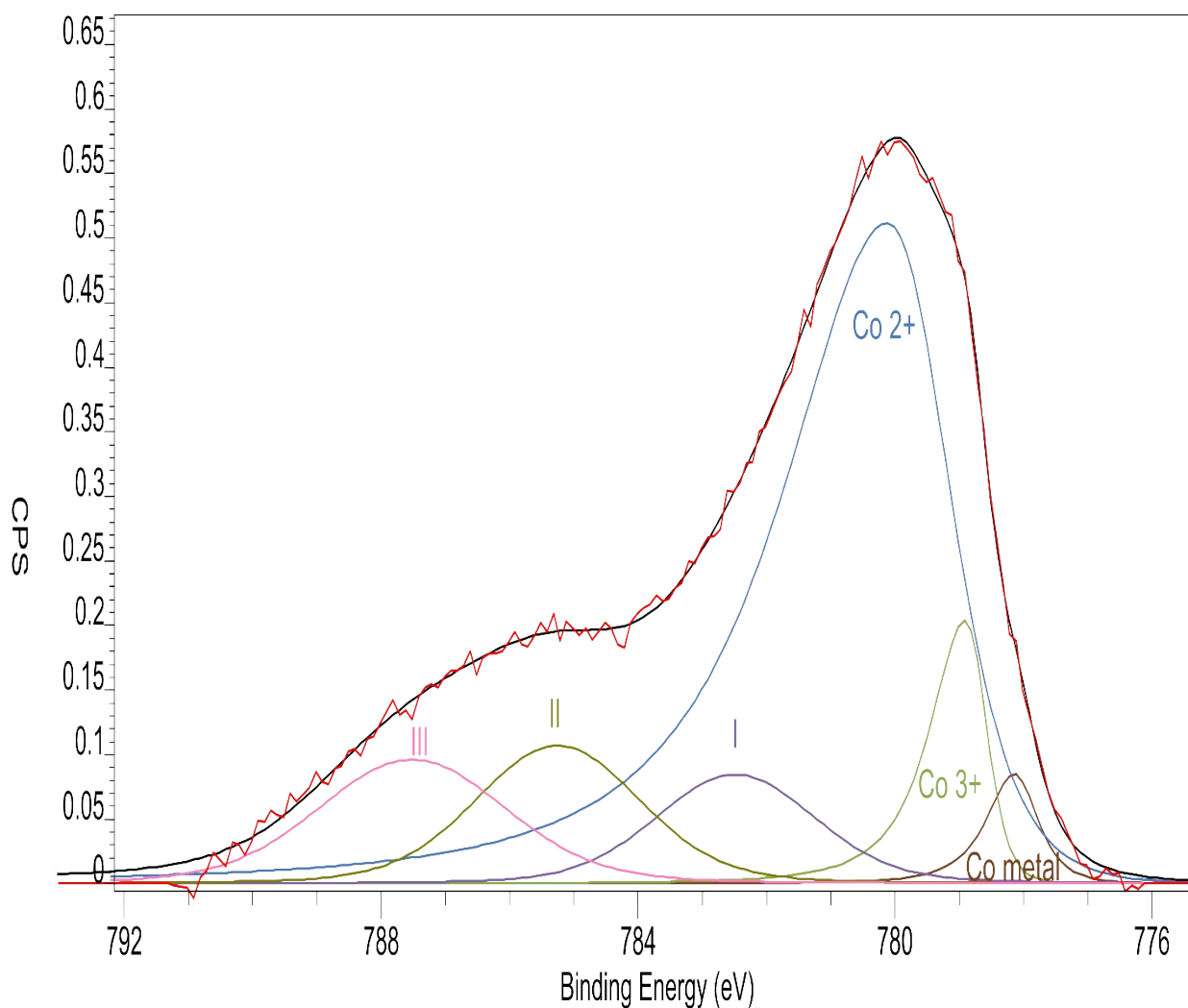


Figure S2 the $\text{Co}2p$ region of the XPS spectra of the CoO_x bilayer, fitted using CASAXPS. The spectra was taken in CO oxidation conditions (2 mbar CO and O_2 in a 1:1 ratio) at 100°C .

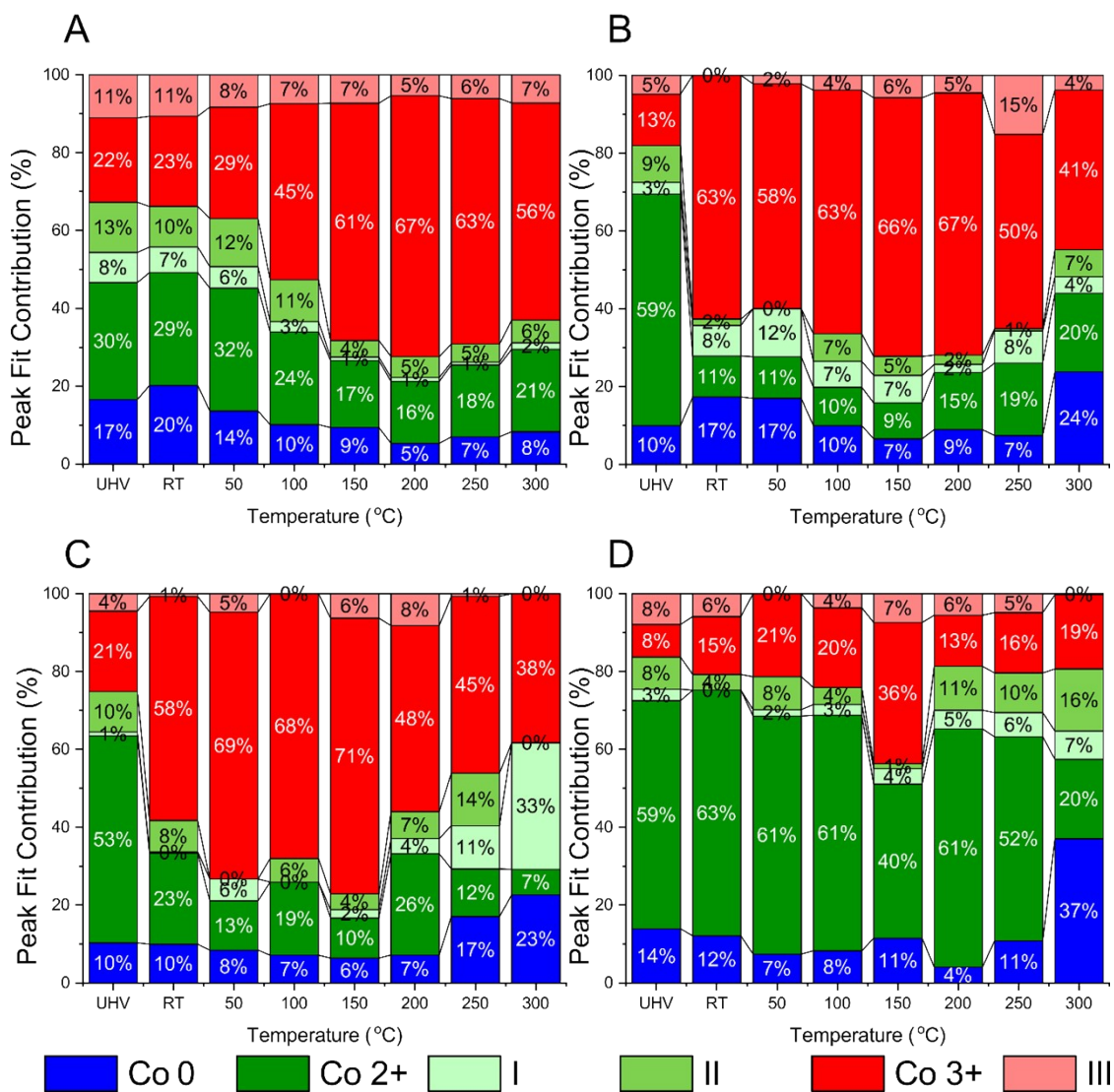


Figure S3. Co_{2p} peak fitting results. Each sub-image shows an experimental series, where the original 0.5ML bilayer is heated in operando conditions. The bar charts show the percentage contribution to the peak fit for the Co_{2p}^{3/2} region of the CoO_x nanoislands XPS spectra. A: CO Oxidation series, B: in PROX conditions H₂:CO:O₂ = 0.1:1:1, C: in PROX conditions H₂:CO:O₂ = 1:1:1, D: in PROX conditions H₂:CO:O₂ = 10:1:1.

Section 3. C1s fitting

Fitting of the C1s region was performed with a purpose written python script. The energy calibration was performed using the Pt 4f^{5/2} peak, measured at each temperature interval using the same photon energy as the C1s region. The peaks were then fitted after Shirley background correction¹⁵ using an analytic approximation to the Voigt function in the form of a Gaussian/Lorentzian Product Function¹⁶. A six-peak fit was used, the first two peaks are ascribed to amorphous carbon at 283.8 eV and 284.3 eV, labelled C1 and C2, seen in Figure S4. They may be the result of both sp² and sp³ bonded carbon¹⁷, when there is relatively large amounts of carbon on the surface, but they represent the adventitious carbon on the surface. The next two peaks fitted are the on-top and bridge site adsorption of CO on the Pt(111), as also seen in Figure S1, at 286.5eV and 285.8eV respectively. The last two peaks fitted were carbonates species peaks, assigned as the on-top and bridge site adsorption of CO on the CoOx nanoislands. These are labelled α and β in the main text, with centres at at 288.4eV and 287.7eV. These are ascribed with the similarities to in binding energies to CoCO₃¹⁸ and to CO on metal oxide surfaces¹⁹ in mind. Shown in Figure S4 are the areas of each of the fitted peaks (calculated using the numpy.trapz function), over the course of the temperature series, in each of the different gaseous environments.

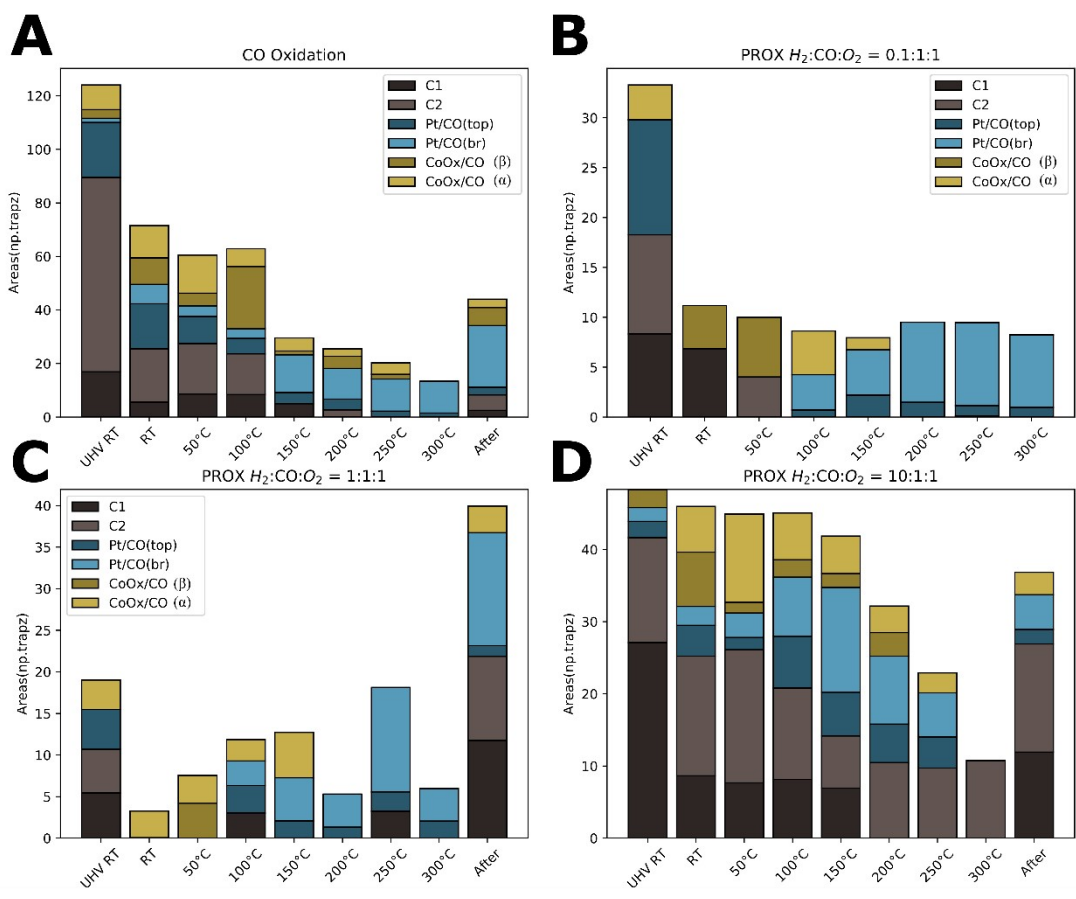


Figure S4 the areas of the fitted surface peaks in the C1s region of the course of the temperature series for each of the different gaseous environments. **A:** CO oxidation with 2 mbar of a 1:1 mix of CO and O₂. **B:** Low H₂ PROX, 6 mbar of a 1:1:0.1 mix of CO:O₂:H₂. **C:** Equivalent H₂ PROX, 6 mbar of a 1:1:1 mix of CO:O₂:H₂. **D:** High H₂ PROX, 6 mbar of a 1:1:10 mix of CO:O₂:H₂.

Section 4. O1s peak fitting

Fitting of the O1s region was performed with a purpose written python script. The energy calibration was performed using the Pt 4f^{5/2} peak, measured at each temperature interval using the same photon energy as the O1s region. The peaks were then fitted after Shirley background correction¹⁵ using an analytic approximation to the Voigt function in the form of a Gaussian/Lorentzian Product Function¹⁶. One of the difficulties with fitting the O1s region arises when you consider there is the potential to fit seven peaks to the region. These peaks begin at lower binding energy with the lattice oxygen of the CoOx at 529.4eV as well as a hydroxyl peak at 531.1eV^{20,21}. Between those two peaks there may also be a chemisorbed oxygen peak (O_{ads}),⁵ however as seen in S1, this peak may also be related to the bridge site adsorption of CO on the Pt(111), shifted to lower binding energy due to the presence of oxygen on the surface. The same can be said of the on-top adsorption sight seen at 532.5eV but reported at 532.9eV in a pure CO environment². Further still, we know that the CO adsorbs on the on-top and bridge sites of the CoOx from the C1s region of the spectra. This adsorption has been reported in literature as having a binding energy of that overlaps the hydroxyl region at 531.1eV²², while Ferstl et al states that at low temperatures on Co₃O₄ a peak at approx. 534eV is the a result of CO bonding to the Co²⁺ sites¹⁷. However when trying to fit so many peaks the representation in the deconvolution was lost, that is without better resolution in the energy axis peaks would be favoured over others in the automated fitting in a non-consistent manner. This can be qualitatively seen when looking at the O1s regions presented in the main text, without a fitting graphed, that it is difficult to assign more than three peaks at any one time. With this in mind a peak fit of four peaks was chosen. As seen in Figure S5 these peaks were the main CoOx lattice peak, the –OH hydroxyl peak which overlaps with a CO adsorption peak on CoOx, the O_{ads} peak which can also overlap with the CO on Pt bridge site, and the CO on Pt top site. The areas of these peaks were graphed in the same way as in Figure S4, and

while they do give an indication of the surface chemistry, the complexity makes further deconvolution and true quantitative analysis difficult.

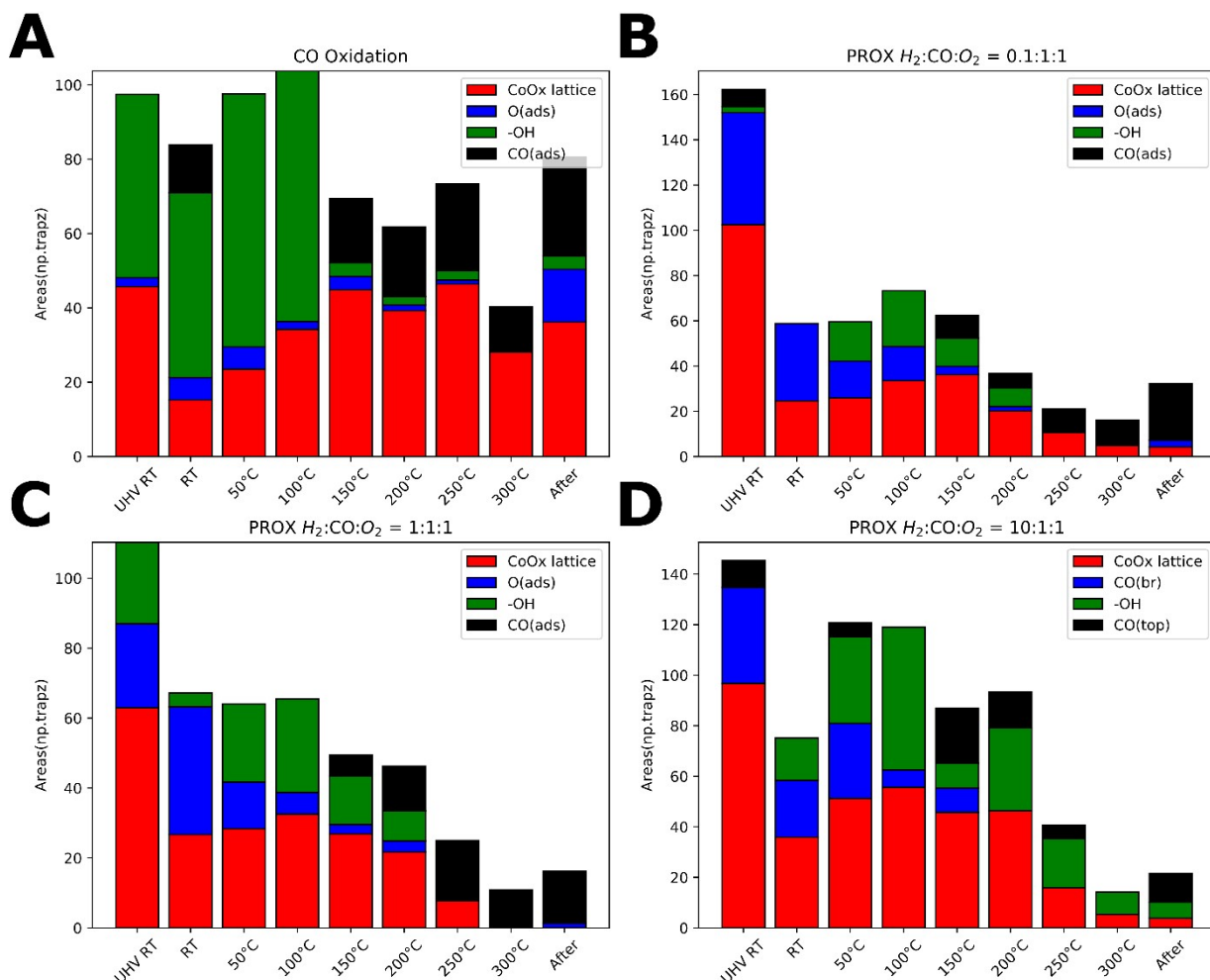


Figure S5 the areas of the fitted surface peaks in the O1s region of the course of the temperature series for each of the different gaseous environments. **A:** CO oxidation with 2 mbar of a 1:1 mix of CO and O₂. **B:** Low H₂ PROX, 6 mbar of a 1:1:0.1 mix of CO:O₂:H₂. **C:** Equivalent H₂ PROX, 6 mbar of a 1:1:1 mix of CO:O₂:H₂. **D:** High H₂ PROX, 6 mbar of a 1:1:10 mix of CO:O₂:H₂.

Another interesting result from Ferstl et al was noting that the main peak of the oxygen lattice site shifted to lower binding energy in the presence of CO, from 529.5eV to 529.35eV. At 150°C, the temperature of light-off of the CO₂ we see the CoOx lattice oxygen peak shift back towards the accepted value of 529.4eV, and raising in binding energy further as more of it is reduced away.

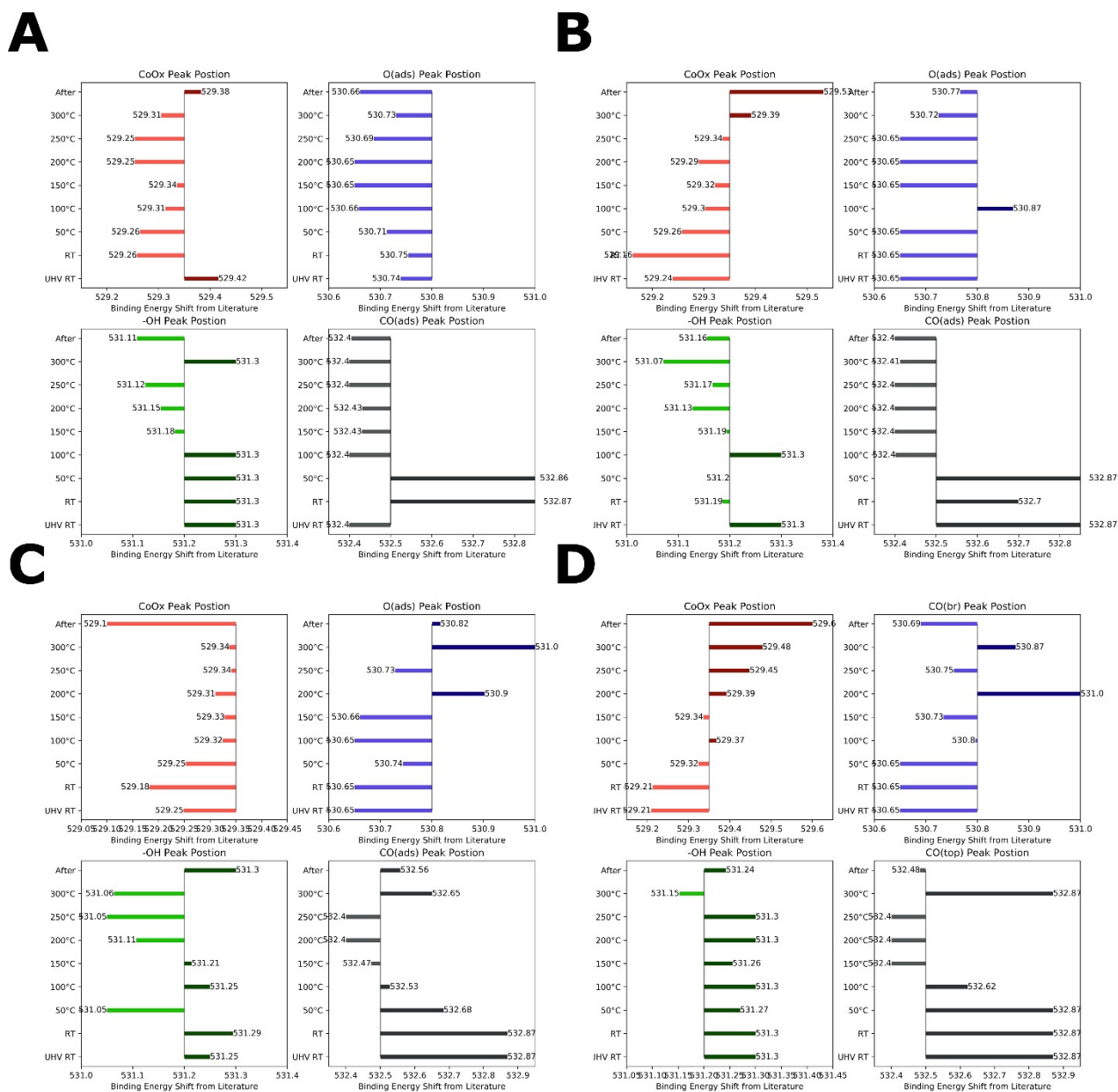


Figure S6 the shift in Binding energy from literature of the fitted surface peaks in the O1s region of the course of the temperature series for each of the different gaseous environments. **A:** CO oxidation with 2 mbar of a 1:1 mix of CO and O₂. **B:** Low H₂ PROX, 6 mbar of a 1:1:0.1 mix of CO:O₂:H₂. **C:** Equivalent H₂ PROX, 6 mbar of a 1:1:1 mix of CO:O₂:H₂. **D:** High H₂ PROX, 6 mbar of a 1:1:10 mix of CO:O₂:H₂.

References

- (1) Pérez-Dieste, V.; Aballe, L.; Ferrer, S.; Nicolàs, J.; Escudero, C.; Milán, A.; Pellegrin, E. Near Ambient Pressure XPS at ALBA. *J. Phys. Conf. Ser.* **2013**, *425* (7), 072023. <https://doi.org/10.1088/1742-6596/425/7/072023>.
- (2) Toyoshima, R.; Yoshida, M.; Monya, Y.; Suzuki, K.; Amemiya, K.; Mase, K.; Mun, B. S.; Kondoh, H. A High-Pressure-Induced Dense CO Overlayer on a Pt(111) Surface: A Chemical Analysis Using in Situ near Ambient Pressure XPS. *Phys. Chem. Chem. Phys.* **2014**, *16* (43), 23564–23567. <https://doi.org/10.1039/C4CP04318A>.
- (3) Blomberg, S.; Hoffmann, M. J.; Gustafson, J.; Martin, N. M.; Fernandes, V. R.; Borg, A.; Liu, Z.; Chang, R.; Matera, S.; Reuter, K.; Lundgren, E. In Situ X-Ray Photoelectron Spectroscopy of Model Catalysts: At the Edge of the Gap. *Phys. Rev. Lett.* **2013**, *110* (11), 117601. <https://doi.org/10.1103/PhysRevLett.110.117601>.
- (4) Avval, T. G.; Chatterjee, S.; Hodges, G. T.; Bahr, S.; Dietrich, P.; Meyer, M.; Thißen, A.; Linford, M. R. Oxygen Gas, O₂ (g), by near-Ambient Pressure XPS. *Surf. Sci. Spectra* **2019**, *26* (1), 014021. <https://doi.org/10.1116/1.5100962>.
- (5) van Spronsen, M. A.; Frenken, J. W. M.; Groot, I. M. N. Observing the Oxidation of Platinum. *Nat. Commun.* **2017**, *8* (1), 429. <https://doi.org/10.1038/s41467-017-00643-z>.
- (6) Völkening, S.; Wintterlin, J. CO Oxidation on Pt(111)—Scanning Tunneling Microscopy Experiments and Monte Carlo Simulations. *J. Chem. Phys.* **2001**, *114* (14), 6382–6395. <https://doi.org/10.1063/1.1343836>.
- (7) Walton, J.; Wincott, P.; Fairley, N.; Carrick, A. *Peak Fitting with CasaXPS: A Casa Pocket Book*; Accolyte Science: United Kingdom, 2010.
- (8) Holt, A. J.; Pakdel, S.; Rodriguez-Fernandez, J.; Zhang, Y.; Curcio, D.; Sun, Z.; Lacovig, P.; Yao, Y.-X.; Lauritsen, J.; Lizzit, S.; Lanata, N.; Hofmann, P.; Bianchi, M.; Sanders, C. E. Electronic Properties of Single-Layer CoO₂/Au(111). *Rev.* **2021**.
- (9) Walton, A. S.; Fester, J.; Bajdich, M.; Arman, M. A.; Osiecki, J.; Knudsen, J.; Vojvodic, A.; Lauritsen, J. V. Interface Controlled Oxidation States in Layered Cobalt Oxide Nanoislands on Gold. *ACS Nano* **2015**, *9* (3), 2445–2453. <https://doi.org/10.1021/acsnano.5b00158>.
- (10) Fester, J.; Walton, A.; Li, Z.; Lauritsen, J. V. Gold-Supported Two-Dimensional Cobalt Oxyhydroxide (CoOOH) and Multilayer Cobalt Oxide Islands. *Phys. Chem. Chem. Phys.* **2017**, *19* (3), 2425–2433. <https://doi.org/10.1039/C6CP07901F>.
- (11) Frost, D. C.; McDowell, C. A.; Woolsey, I. S. X-Ray Photoelectron Spectra of Cobalt Compounds. *Mol. Phys.* **1974**, *27* (6), 1473–1489. <https://doi.org/10.1080/00268977400101251>.
- (12) Chuang, T. J.; Brundle, C. R.; Rice, D. W. Interpretation of the X-Ray Photoemission Spectra of Cobalt Oxides and Cobalt Oxide Surfaces. *Surf. Sci.* **1976**, *59* (2), 413–429. [https://doi.org/10.1016/0039-6028\(76\)90026-1](https://doi.org/10.1016/0039-6028(76)90026-1).
- (13) Biesinger, M. C.; Payne, B. P.; Grosvenor, A. P.; Lau, L. W. M.; Gerson, A. R.; Smart, R. S. C. Resolving Surface Chemical States in XPS Analysis of First Row Transition Metals, Oxides and Hydroxides: Cr, Mn, Fe, Co and Ni. *Appl. Surf. Sci.* **2011**, *257* (7), 2717–2730. <https://doi.org/10.1016/j.apsusc.2010.10.051>.

- (14) Kim, K. S. X-Ray-Photoelectron Spectroscopic Studies of the Electronic Structure of CoO. *Phys. Rev. B* **1975**, *11* (6), 2177–2185. <https://doi.org/10.1103/PhysRevB.11.2177>.
- (15) Castle, J. .; Chapman-Kpodo, H.; Proctor, A.; Salvi, A. . Curve-Fitting in XPS Using Extrinsic and Intrinsic Background Structure. *J. Electron Spectros. Relat. Phenomena* **2000**, *106* (1), 65–80. [https://doi.org/10.1016/S0368-2048\(99\)00089-4](https://doi.org/10.1016/S0368-2048(99)00089-4).
- (16) Evans, S. Curve Synthesis and Optimization Procedures for X-Ray Photoelectron Spectroscopy. *Surf. Interface Anal.* **1991**, *17* (2), 85–93. <https://doi.org/10.1002/sia.740170204>.
- (17) Leung, T. .; Man, W. .; Lim, P. .; Chan, W. .; Gaspari, F.; Zukotynski, S. Determination of the Sp³/Sp² Ratio of a-C:H by XPS and XAES. *J. Non. Cryst. Solids* **1999**, *254* (1–3), 156–160. [https://doi.org/10.1016/S0022-3093\(99\)00388-9](https://doi.org/10.1016/S0022-3093(99)00388-9).
- (18) Cong, H.-P.; Yu, S.-H. Shape Control of Cobalt Carbonate Particles by a Hydrothermal Process in a Mixed Solvent: An Efficient Precursor to Nanoporous Cobalt Oxide Architectures and Their Sensing Property. *Cryst. Growth Des.* **2009**, *9* (1), 210–217. <https://doi.org/10.1021/cg8003068>.
- (19) Morais, A.; Alves, J. P. C.; Lima, F. A. S.; Lira-Cantu, M.; Nogueira, A. F. Enhanced Photovoltaic Performance of Inverted Hybrid Bulk-Heterojunction Solar Cells Using TiO₂/Reduced Graphene Oxide Films as Electron Transport Layers. *J. Photonics Energy* **2015**, *5* (1), 057408. <https://doi.org/10.1117/1.JPE.5.057408>.
- (20) Fester, J.; Sun, Z.; Rodríguez-Fernández, J.; Walton, A.; Lauritsen, J. V. Phase Transitions of Cobalt Oxide Bilayers on Au(111) and Pt(111): The Role of Edge Sites and Substrate Interactions. *J. Phys. Chem. B* **2018**, *122* (2), 561–571. <https://doi.org/10.1021/acs.jpcc.7b04944>.
- (21) Fester, J.; Bajdich, M.; Walton, A. S.; Sun, Z.; Plessow, P. N.; Vojvodic, A.; Lauritsen, J. V. Comparative Analysis of Cobalt Oxide Nanoisland Stability and Edge Structures on Three Related Noble Metal Surfaces: Au(111), Pt(111) and Ag(111). *Top. Catal.* **2017**, *60* (6–7), 503–512. <https://doi.org/10.1007/s11244-016-0708-6>.
- (22) Kersell, H.; Hooshmand, Z.; Yan, G.; Le, D.; Nguyen, H.; Eren, B.; Wu, C. H.; Waluyo, I.; Hunt, A.; Nemšák, S.; Somorjai, G.; Rahman, T. S.; Sautet, P.; Salmeron, M. CO Oxidation Mechanisms on CoO_x-Pt Thin Films. *J. Am. Chem. Soc.* **2020**, *142* (18), 8312–8322. <https://doi.org/10.1021/jacs.0c01139>.